Remote Sens. **2012**, *4*, 849-866; doi:10.3390/rs4040849

OPEN ACCESS

Remote Sensing

ISSN 2072-4292

www.mdpi.com/journal/remotesensing

Article

Estimating Net Primary Production of Turfgrass in an Urban-Suburban Landscape with QuickBird Imagery

Jindong Wu [1,*] and Marvin E. Bauer [2]

[1] Department of Geography, California State University, Fullerton, 800 North State College Boulevard, Fullerton, CA 92831, USA

[2] Department of Forest Resources, University of Minnesota, 1530 Cleveland Avenue North, Saint Paul, MN 55108, USA; E-Mail: mbauer@umn.edu

* Author to whom correspondence should be addressed; E-Mail: jindongwu@fullerton.edu; Tel.: +1-657-278-4020; Fax: +1-657-278-5223.

Received: 29 January 2012; in revised form: 15 March 2012 / Accepted: 16 March 2012 / Published: 27 March 2012

Abstract: Vegetation is a basic component of urban-suburban environments with significant area coverage. As a major vegetation type in US cities, urban turfgrass provides a range of important ecological services. This study examined the biological carbon fixation of turfgrass in a typical residential neighborhood by linking ground-based measurements, high resolution satellite remote sensing, and ecological modeling. The spatial distribution of turfgrass and its vegetative conditions were mapped with QuickBird satellite imagery. The significant amount of shadows existing in the imagery were detected and removed by taking advantage of the high radiometric resolution of the data. A remote sensing-driven production efficiency model was developed and parameterized with field biophysical measurements to estimate annual net primary production of turfgrass. The results indicated that turfgrass accounted for 38% of land cover in the study area. Turfgrass assimilated 0–1,301 $g{\cdot}C{\cdot}m^{-2}{\cdot}yr^{-1}$ depending on vegetative conditions and management intensity. The average annual net primary production per unit turfgrass cover by golf course grass (1,100.5 $g{\cdot}C{\cdot}m^{-2}$) was much higher than that by regular lawn grass (771.2 $g{\cdot}C{\cdot}m^{-2}$). However, lawn grass contributed more to the total net primary production than golf course grass due to its larger area coverage, although with higher spatial variability.

Keywords: urban vegetation; modeling; carbon cycle; high resolution

1. Introduction

Half of the global population now lives in urban areas and the world urban population is expected to double by 2050 [1]. As a major component of land transformation processes, urbanization driven by population growth is apparent in many parts of the world. Urban areas continue to expand at unprecedented rates with a projected increase of 22 million hectares in the US between 2003 and 2030 [2]. As a matter of fact, the urban expansion has outpaced population growth across the US [2,3]. However, the consequences of urban and suburban development for human health and ecosystem functions remain largely elusive [4].

Vegetation is a basic component of urban-suburban environments with significant area coverage. It was estimated that urban forest in the US contains approximately 3.8 billion trees with an average tree canopy cover of 27% [5], and turfgrass in the continental US occupies 163,800 km^2, an area three times larger than the surface of any irrigated crop [6]. Urban trees and grass provide a full range of ecosystem services that are vital to human health [7] and environmental quality [8]. Urban vegetation has the potential to affect local climate [9], reduce air pollution [10], mitigate storm-water runoff and improve ground water quality [11], as well as provide habitat for wildlife [12].

Another ecosystem service that is increasingly important is the biological carbon uptake of urban vegetation in relation to climate change mitigation policies. Terrestrial vegetation acts as one of the potential carbon sinks through photosynthesis. Considerable research has been directed in recent years at terrestrial carbon balance of forests, grasslands, and agricultural lands, but only a few studies have included urban and suburban landscapes to quantify and map carbon budget of urban vegetation [13−15]. This is likely due to the perception that urban areas are relatively small in size compared with other terrestrial surfaces [16] and play an insignificant role in the global carbon cycle.

Although urban areas occupy a relatively small fraction (<3%) of Earth's terrestrial surface, the size of urban carbon reservoirs appears to be substantial [4]. One study estimated that carbon storage by urban trees in US cities is equivalent to the amount of carbon emitted by Americans in about 5.5 months [17]. Quantification of the contribution of urban vegetation to regional carbon budget is important for understanding and mitigating many aspects of carbon sinks and sources and global climate change [18,19]. Studies have shown that low density suburban areas, which are prevalent around many metropolitan regions and characterized by large proportions of vegetation, can be more productive than non-urban forest, native grasslands, and cultivated lands; thus at regional scale, carbon uptake from the atmosphere may be strengthened as a result of the rural land conversion [17,20,21] though urban development may have largely reduced the productivity of the land surface at continental scale [22]. Reliable methods and high resolution data are needed to help local agencies to facilitate the development of successful carbon management programs for monitoring and reducing urban carbon emission.

Ecological studies of carbon cycling in urban plants have only begun with the majority of effort on carbon storage by urban vegetation [17,23–25]. Most of these studies have been restricted to inventories of urban vegetation on public lands. The estimated average carbon storage by urban trees in 10 US cities was 2.51 $kg \cdot C \cdot m^{-2}$ of urban area based on the national urban tree inventory data and allometric equations [17]. This approach has provided a wealth of valuable data, but only a small fraction of the area of interest can be surveyed since field measurements are labor intensive and expensive, and

not all patches of vegetation within an urban landscape can be accounted for. Additionally, it is difficult to strictly adhere to a specific sampling design in landscape level inventory studies (e.g., permission to access private properties) and the methods used are not always consistent [20]. Therefore, it is difficult to compare the estimates generated from different studies. The estimates become more uncertain when extrapolating from individual field plots to assess urban carbon at the state, regional, and national levels [17].

Although much effort has been directed to the carbon storage of urban vegetation, only a few studies have attempted to estimate the temporal dynamics of carbon fixation. In the limited studies available, the estimated annual net primary production (NPP) of turfgrass varies greatly although it is generally agreed that turfgrass acts as a carbon sink [6,20,26,27].

The key to successful estimation of carbon budgets of urban-suburban ecosystems is determining the composition of landscapes in terms of land use and land cover and vegetation conditions. Remotely sensed imagery provides a unique synoptic view of the Earth's environment without labor intensive and exhaustive field surveys. It has been widely recognized that satellite observations of the Earth's surface can be used to document land use and land cover over large areas. The estimation of carbon budgets with remotely sensed imagery, however, becomes difficult in urban-suburban areas because of increased spatial heterogeneity and the relatively low resolution of imagery data [6]. Given the high spatial heterogeneity of urban landscapes, land cover can change in short distances and all can occur in a small area. Traditional urban land use and land cover schemes, which include categories such as residential, commercial, and transportation, do not adequately resolve landscapes to include detailed vegetation information [28]. The accuracy of turfgrass NPP estimates is therefore limited by the uncertainty in mapping the area coverage.

High spatial resolution remote sensing provides significant opportunities to detect fine details on the ground. With high resolution imagery, all turfgrass in residential, institutional, and commercial lawns, parks, athletic fields, and golf courses, etc. can be accounted for. The information derived from high resolution imagery is at the scale and resolution most pertinent for urban landscape planning and management [29]. However, extensive shadows also exist in high resolution images and create problems in directly applying imagery data to urban land use and land cover classification [30]. Shadowed areas are traditionally left unclassified or simply classified as shadows. As a result, a significant portion of land cover including vegetation coverage is lost in the classification, and thus the vegetative carbon fixation by turfgrass is most likely underestimated.

Considerable remote sensing based ecological carbon studies have employed production efficiency models (PEM) in quantifying carbon budgets of natural ecosystems and croplands [31–35]. PEMs are often driven by a relatively constant relationship between photosynthetic carbon fixation and radiation received at the canopy level. The radiation received at the canopy level is commonly estimated through the fraction of absorbed photosynthetically active radiation (fAPAR), which is the fraction of incoming solar radiation in the PAR spectral region that is absorbed by photosynthetic organisms. However, these models cannot be directly applied to urban turfgrass because of its unique canopy structure and biophysical characteristics. Additionally, considering the canopy height of turfgrass (<15 cm), it remains difficult to measure fAPAR of turfgrass canopies with traditionally used PAR ceptometers.

The objectives of this study were (1) to map and estimate the spatial distribution and vegetative condition of turfgrass at local scale by resolving shadows in QuickBird satellite images, (2) to develop

a remote sensing-driven PEM and parameterize the fAPAR for turfgrass canopies with field biophysical measurements, and (3) to quantify the annual NPP of turfgrass with the PEM under different management practices, such as varying nitrogen fertilization regimes.

2. Methods

2.1. Study Area and Data Collection

The study area is a suburban residential neighborhood (15.5 km^2, northwest corner: 45°0′40″N, 93°12′40″W; southeast corner: 44°58′32″N, 93°9′42″W), located in Falcon Heights and Roseville, MN, USA. Land use and land cover of the study area is dominated by high-density residential development, but also includes commercial and institutional land development such as industrial buildings, parking lots, highways, trees, and turfgrass. Agricultural research fields of the University of Minnesota are also located in the study area but were masked because the land use is not typical of those in urban-suburban environments.

QuickBird satellite images were acquired for the study area. A set of biophysical variables, including canopy multispectral reflectance, and incoming and reflected PAR, were measured in the field experiments to investigate the dynamics of turf ecosystems with different nutrient conditions. Spectral reflectances were also measured for shadowed surfaces to investigate whether shadows were spectroradiometrically different. Weather and soil conditions were recorded simultaneously.

2.1.1. Satellite Image Acquisition

Two QuickBird multispectral images were acquired on 18 August 2003 and 26 July 2006 under clear sky conditions. The images, with 11-bit radiometric resolution, have three visible bands (0.45–0.52 μm, 0.52–0.60 μm, and 0.63–0.69 μm) and one near infrared band (0.76–0.90 μm). The spatial resolution of the 2003 image was 2.8 m, taken at a sun elevation angle of 54.5°, an off-nadir view angle of 12.1°, and a target azimuth of 111°, while that of the 2006 image was 2.4 m, taken at a sun elevation angle of 62.6°, an off-nadir view angle of 18.2°, and a target azimuth of 90°. The different illumination and viewing geometry at acquisition led to different shadows in the two images. The land use and land cover classification was conducted on the 2006 image, while the 2003 image was used as ancillary data to aid in the classification of shadows when labeling shadow classes. The images were geometrically rectified and radiometrically and atmospherically corrected to obtain surface reflectance [36].

2.1.2. Spectral Reflectance Measurement

Surface spectral reflectances were measured for turfgrass canopies and shadowed surfaces with a 16-band multispectral radiometer (CROPSCAN MSR-16R, 0.46–1.72 μm). The band widths of the spectroradiometer vary from 6.8 nm to 12 nm in the visible and from 11 nm to 13 nm in the near infrared. Both irradiance and radiance were measured simultaneously to derive surface reflectance. The four multispectral bands of QuickBird data were simulated with appropriate CROPSCAN bands as weighted averages (Table 1) [36]. The view angle of the spectroradiometer was constant by looking vertically downward with a 28° field of view (FOV). Measurements were made at 1 m above either

grass canopies or shadowed surfaces, which resulted in a projected view area with a 0.5 m diameter. All reflectance measurements were taken within one hour of solar noon to minimize the effect of diurnal changes in solar zenith angle.

Table 1. QuickBird spectral bands and the corresponding bands of CROPSCAN MSR-16R radiometer.

QuickBird		CROPSCAN Bands (μm)
Bands	**λ (μm)**	
Blue	0.45–0.52	0.4566–0.4634, 0.5062–0.5139
Green	0.52–0.60	0.5553–0.5647
Red	0.63–0.69	0.6540–0.6660
Near IR	0.76–0.90	0.7545–0.7655, 0.8045–0.8155, 0.8640–0.8760, 0.8935–0.9065

The turfgrass canopy reflectance measurements were conducted in the experimental plots at the University of Minnesota Turfgrass Research, Outreach, and Education Center (44°59′N, 93°11′W), located in the study area. The 24 experimental plots consisted of eight nitrogen, phosphate, potassium, and clipping treatments (Table 2). Randomized complete blocks with three replications were used for the experiments. Each plot was 2.44 × 7.32 m and planted with Kentucky bluegrass, a common turfgrass in the United States, on the Waukegan silt loamy soil (fine-silty over sandy mixed Typic Hapludolls) with 3.6% organic matter for the top 15 cm. Six measurement campaigns were carried out in the growing season of 2006. Three random sampling areas were measured within each treatment plot. Measurements were then averaged for each plot.

Table 2. Data collection of multispectral reflectance measured with CROPSCAN MSR-16R and photosynthetically active radiation (PAR) measured with ACCUPAR LP-80.

		No. Plots	**Readings Per Plot**	**Readings Per Measurement Campaign**	**No. Measurement Campaigns**
Reflectance (%)	Turfgrass Canopies	24	3	72	6
	Shadowed Surfaces	37	3	111	1
PAR ($\mu mol \cdot m^{-2} \cdot s^{-1}$)	Turfgrass Canopies	24	1 (upward) 3 (downward)	96	6

Shadowed surface reflectances were measured on 26 September 2006 for both shadows on impervious surfaces (SOI) and shadows on grass (SOG). Thirty seven shadowed plots were selected in the study area, in which 18 were SOI plots and 19 were SOG plots. Each type of shadow (*i.e.*, SOI and SOG) was further divided into shadows cast by buildings (8 for SOI and 7 for SOG) and shadows cast by trees (10 for SOI and 12 for SOG), respectively. Three random sampling areas were selected within each shadowed plot. Measurements were then averaged for each plot to estimate multispectral reflectance values for each type of shadow.

2.1.3. Photosynthetically Active Radiation Measurement

fAPAR was estimated indirectly through incoming and reflected PAR; both were measured with an ACCUPAR LP-80, a linear PAR ceptometer consisting of an integrated probe that contains 80 PAR

photodiodes and a microcontroller. PAR measurements were conducted simultaneously in the same turfgrass experimental plots as the canopy reflectance measurements (Table 2). For each of the 24 plots, PAR measurements consisted of one upward looking (*i.e.*, incoming PAR) and three downward looking acquisitions (*i.e.*, reflected PAR), with the ceptometer being placed at 1 m height. Measurements were averaged for each plot. The PAR measurements were repeated six times in the growing season of 2006.

2.1.4. Meteorological Data

Meteorological data were taken from the University of Minnesota Climatological Observatory's daily observations; it is also located within the study area. Climate normals were also obtained from the same dataset. The data include solar radiation, maximum and minimum air temperature, precipitation, and soil temperature at 5 cm depth. The climate of the study area is continental with large seasonal temperature variations. The coldest month is January when the average monthly minimum temperature can decrease to −14 °C, while in July, the warmest month, the average monthly maximum temperature can rise to 28 °C. The major period of the growing season is from late April to early October with a median growing season of 160 days. The average daily air temperature during this period of time is about 17 °C while the maximum air temperature can be above 30 °C. Approximately 70% of annual precipitation (about 820 mm) occurs during the growing season.

2.2. Shadow Detection and Removal in the Land Use and Land Cover Classification Map

A multi-stage image classification scheme was developed. To reduce the spectral confusion between water and shadows, water cover in the QuickBird image was masked with the Ramsey County open water outlines, which were derived from 2003 aerial orthophotography utilizing stereo processing techniques. Unsupervised ISODATA clustering was then initially used to map major land use and land cover types including impervious surfaces, water, bare soil, crops, trees, and turfgrass. However, one of the spectral classes was inevitably shadows. Measured spectral reflectances of different types of shadow were analyzed to investigate whether shadows were spectroradiometrically different, particularly, in the QuickBird spectral bands. For the purpose of this study, we were more interested in the land cover shaded by shadows than the land cover that casts the shadows. Thus, shadows were grouped into two types: SOI and SOG, regardless of being cast by buildings or by trees. Shadow pixels were also extracted from the QuickBird images to compare spectroradiometric differences between SOI and SOG. Based on these differences, shadow pixels were reclassified to different information classes, *i.e.*, impervious surfaces or grass.

To assess the accuracy of shadow detection and overall classification, Ramsey County color aerial orthophotography (collected on 9 April 2006, spatial resolution, 0.15 m) was used as the reference image. Three hundred points were selected using stratified random sampling with a minimum 30 points for each class. The overall accuracy and producer's and user's accuracies of each class were computed as well as Kappa statistics.

2.3. Shadow Detection and Removal in the QuickBird Images

For the estimation of vegetation conditions and quantification of NPP, it is necessary to restore the spectral information of shadow areas in the original QuickBird imagery. Shadow pixels in the satellite images were first identified by overlaying with the shadow-free classification map. To restore spectral information of shadow areas in the QuickBird imagery, the *k*-nearest neighbor algorithm (k = 1) was applied to resample digital numbers for all shadow pixels [37]. The neighborhood of the shadow pixels was confined to the corresponding information classes, *i.e.*, either grass or impervious surfaces. Through this process, the digital number of the closest pixel within the confined neighborhood was used to replace the original value of the corresponding shadow pixel. The shadow detection and removal were conducted separately for each of the four spectral bands of the QuickBird images.

2.4. Net Primary Production Modeling

A remote sensing-driven PEM model was developed to estimate NPP of turfgrass:

$$NPP = \varepsilon \times fAPAR \times PAR \tag{1}$$

$$fAPAR = a \times NDVI + b \tag{2}$$

$$\varepsilon = f(T_a, T_s) \times \varepsilon_{max}(N) \tag{3}$$

$$f(T_a, T_s) = \begin{cases} 0 & T_a \le 0°\text{C}, T_a \ge 40°\text{C}, \text{or } T_s \le 0°\text{C} \\ \dfrac{(T_a - T_{min})(T_a - T_{max})}{(T_a - T_{min})(T_a - T_{max}) - (T_a - T_{opt})^2} & 0°\text{C} < T_a < 40°\text{C} \text{ and } T_s > 0°\text{C} \end{cases} \tag{4}$$

where NPP is the net primary production, *i.e.*, the total amount of carbon fixed by turfgrass through the process of photosynthesis after the costs of plant respiration ($g \cdot C \cdot m^{-2}$); ε is the light use efficiency ($g \cdot C \cdot MJ^{-1}$); $\varepsilon_{max}(N)$ is the maximum light use efficiency under optimal growth conditions ($g \cdot C \cdot MJ^{-1}$) at a certain nitrogen level; it was derived from *in situ* measurements of net canopy photosynthesis and light and nitrogen conditions [38,39]. a and b are the slope and intercept of the regression line between fAPAR and normalized difference vegetation index (NDVI), respectively. $f(T_a,T_s)$ is a scale factor controlled by environmental stresses for air temperature (T_a), soil temperature at 5 cm (T_s), and the maximum (T_{max}), minimum (T_{min}), and optimal temperature (T_{opt}) for Kentucky bluegrass to grow.

Biophysical measurements in the controlled experimental plots were used to parameterize fAPAR. As mentioned before, it is difficult to measure fAPAR of turfgrass canopies directly because of the short and tight canopies. We developed a simplified coupled leaf/canopy radiative transfer model and inverted it to estimate turfgrass canopy fAPAR with field-measured incoming and canopy reflected PAR, and leaf and soil reflectances in the PAR spectral region. The model was simplified by considering only two layers of turfgrass leaves and one layer of soil and assuming turfgrass canopies are horizontally homogeneous and laterally infinite. NDVI values were computed with weighted average canopy reflectance measurements in corresponding wavelengths (Table 1) [40].

The scale factor was determined by a piecewise function on the basis of T_a and T_s. If T_a and T_s were within the acceptable temperature range, $f(T_a,T_s)$ was calculated with a scale normalization function by

comparing T_s with the three threshold temperatures for turfgrass growth. Otherwise, $f(T_a,T_s)$ was given a value of zero, meaning that no carbon would be assimilated under this environmental condition.

Turfgrass in the study area is generally well-watered. Three nitrogen levels were considered to indicate the intensity of management: high ($\varepsilon_{max}(N)$ = 1.08 g·C·MJ^{-1}), medium ($\varepsilon_{max}(N)$ = 0.84 g·C·MJ^{-1}), and low ($\varepsilon_{max}(N)$ = 0.65 g·C·MJ^{-1}). High nitrogen level denotes multiple fertilizer applications throughout the year; medium nitrogen level represents use of fertilizers only once or twice per year; and low nitrogen level has no fertilizer application. Three NDVI threshold values were selected to correspond with each nitrogen level based on the examination of the histogram of the NDVI imagery and field survey. High or low nitrogen level was denoted if NDVI value was greater than 0.8 or less than 0.5, respectively. Medium nitrogen level was denoted if NDVI was between 0.5 and 0.8. The calculations were based on the simplified assumption that, under a given nitrogen scenario, turfgrass within the corresponding NDVI range was fertilized with the same amount of nitrogen. This way, the PEM model responds to both the spatial heterogeneity of turfgrass implicit in the satellite data and management practices.

Using the shadow-free high resolution land use and land cover map, the shadow-free QuickBird images, and the local climate and soil data as the inputs, the parameterized PEM was implemented to estimate turfgrass NPP for the entire study area. We implemented the PEM for other times of the growing season when satellite images were not available under the assumption that the vegetation properties derived from the acquired satellite data represented the typical turfgrass condition throughout the growing season. The modeled results were integrated over the whole growing season to provide a map of the total annual NPP at 2.4 m spatial resolution.

3. Results

3.1. Land Use and Land Cover

A high resolution (2.4 m) land use and land cover map was derived from the classification of QuickBird imagery when shadow pixels were reclassified to different information classes (Figure 1). Golf course grass was spectrally significantly different from regular lawn grass, and thus was classified separately. The QuickBird image classification indicated that shadows accounted for about 7% of total land cover in the study area (Figure 2). Different types of shadow (*i.e.*, SOI and SOG) had distinct spectral characteristics, particularly in the near infrared wavelengths (Figure 3). Based on these differences, the SOI and SOG were successfully separated (Figure 3), and the shadow areas were reclassified to the corresponding information classes (Figure 2).

The overall classification accuracy was 84% with overall Kappa statistics of 0.81 (Table 3). The producer's and user's accuracies of vegetation classes were in the range of 80–85%, which were slightly lower than the 84–89% accuracy achieved for the impervious surfaces. SOG was detected with the highest producer's accuracy (90%) while SOI was detected with the highest user's accuracy (94%) among all classes. However, SOI was defined more accurately than SOG after accounting for chance agreement, probably due to the low spatial variation of SOI (Figure 3).

The shadow-free classification showed that urban vegetation accounted for about 60% of the land surface in this residential neighborhood, with about 38% being turfgrass (Figure 2). Spectral information

was also correspondingly restored for shadow areas in the original QuickBird images. Figure 4 illustrates the results of shadow removal in the original QuickBird images covering the same area as shown in the land cover maps (Figure 5).

Figure 1. The location of the study area within the state of Minnesota and its land use and land cover types derived from QuickBird imagery and aerial orthophotography after shadow areas were reclassified to information classes.

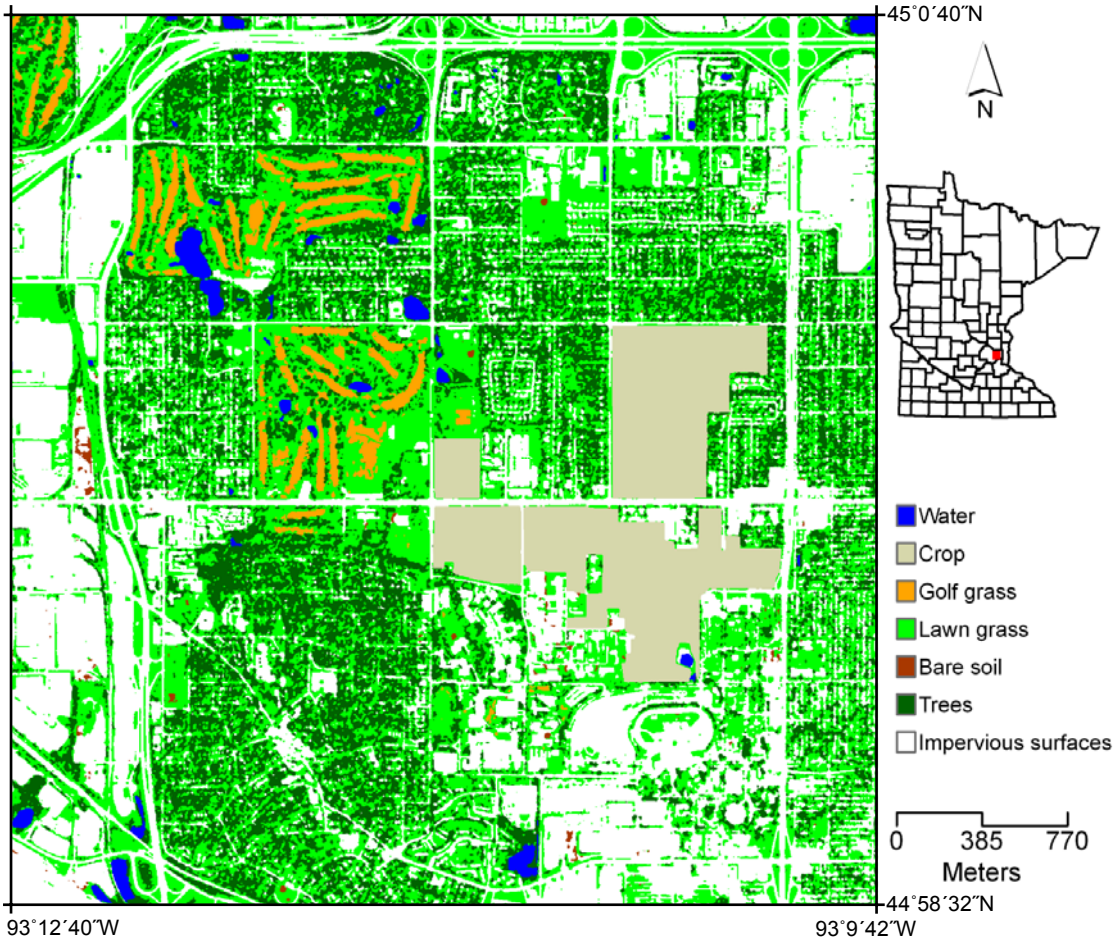

Figure 2. Percentages of land use and land cover by type classified with QuickBird imagery before and after the shadows in the images were detected and removed.

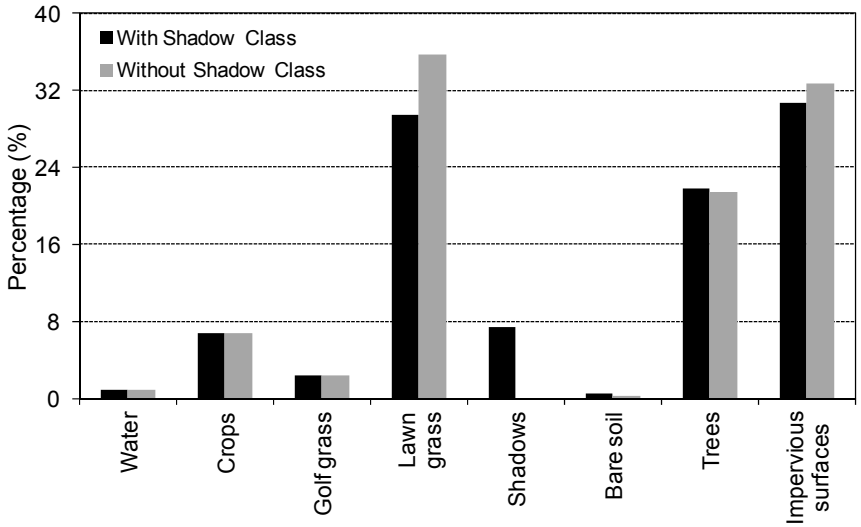

Figure 3. Multispectral reflectances of shadows measured with CROPSCAN radiometer on grass (SOG) (n = 57) and on impervious surfaces (SOI) (n = 54), cast either by buildings or trees (**left**). The spectroradiometric differences between SOG and SOI are also shown in the digital numbers of sampled shadow pixels in the QuickBird images (n = 65) (**right**). The vertical lines indicate the range of variability in each spectral band of QuickBird imagery.

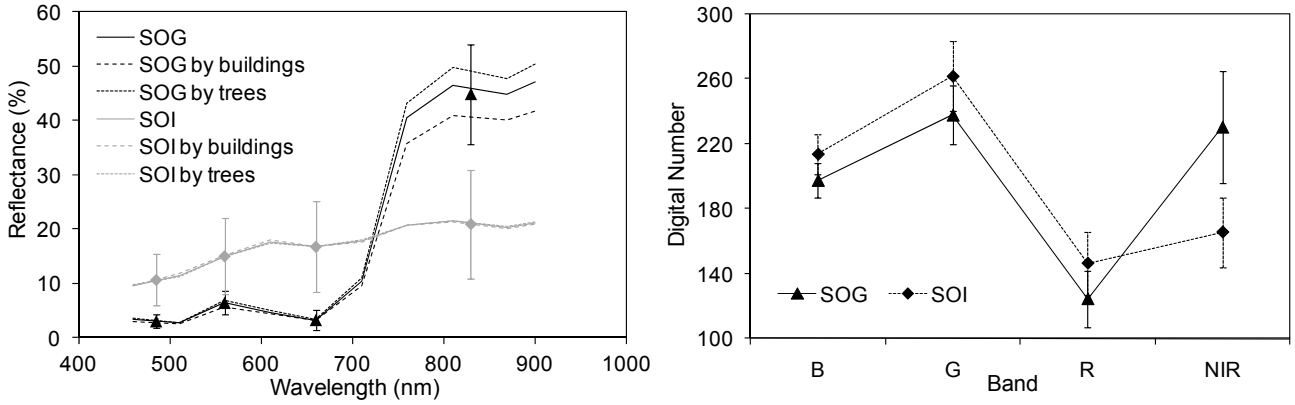

Table 3. Accuracy assessment of shadow detection and land use and land cover classification. SOG and SOI refer to shadows on turfgrass and shadows on impervious surfaces, respectively.

Class	Producer's Accuracy	User's Accuracy	Kappa
Turfgrass	82.1	79.7	0.76
Trees	80.7	85.2	0.81
Impervious Surfaces	84.4	88.5	0.85
Bare Soil	87.5	75.0	0.78
SOG	90.0	73.0	0.75
SOI	78.4	93.6	0.93

Figure 4. QuickBird false color images before shadows were removed (**left**) and after spectral information was restored for shadow pixels (**right**).

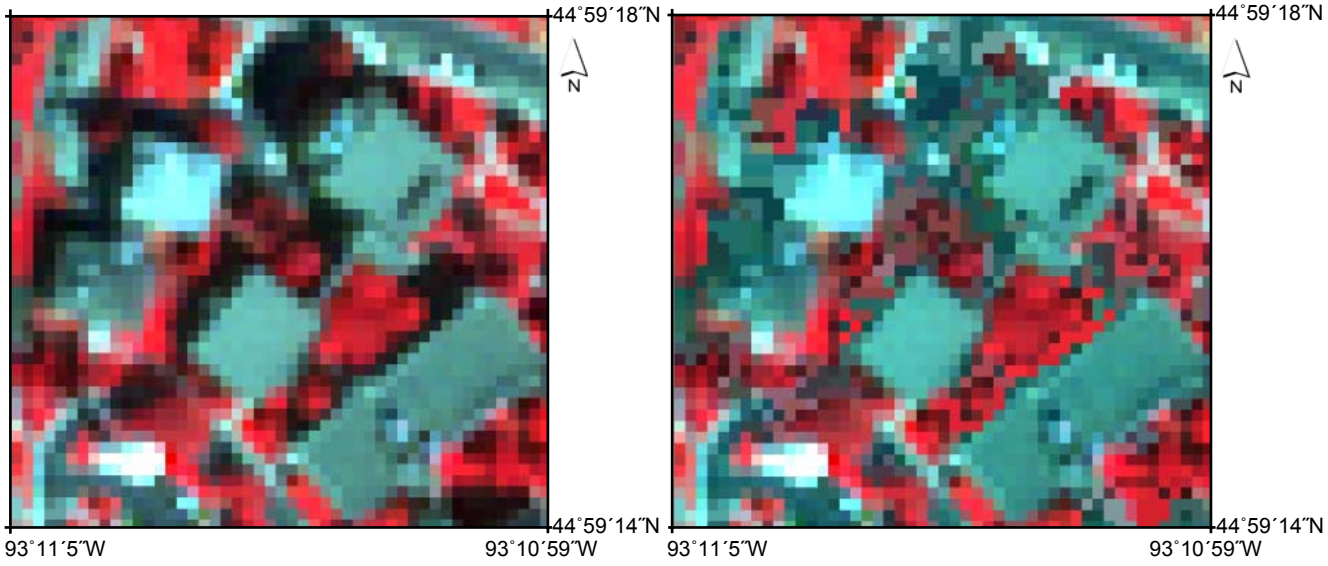

Figure 5. Land use and land cover maps before (**left**) and after (**right**) shadow areas were removed. Areas in gray are shadows on grass (SOG) while areas in black are shadows on impervious surfaces (SOI). SOG and SOI were reclassified to grass (green) and impervious surfaces (white), respectively. Dark green and brown colors represent areas covered by trees and bare soil, respectively.

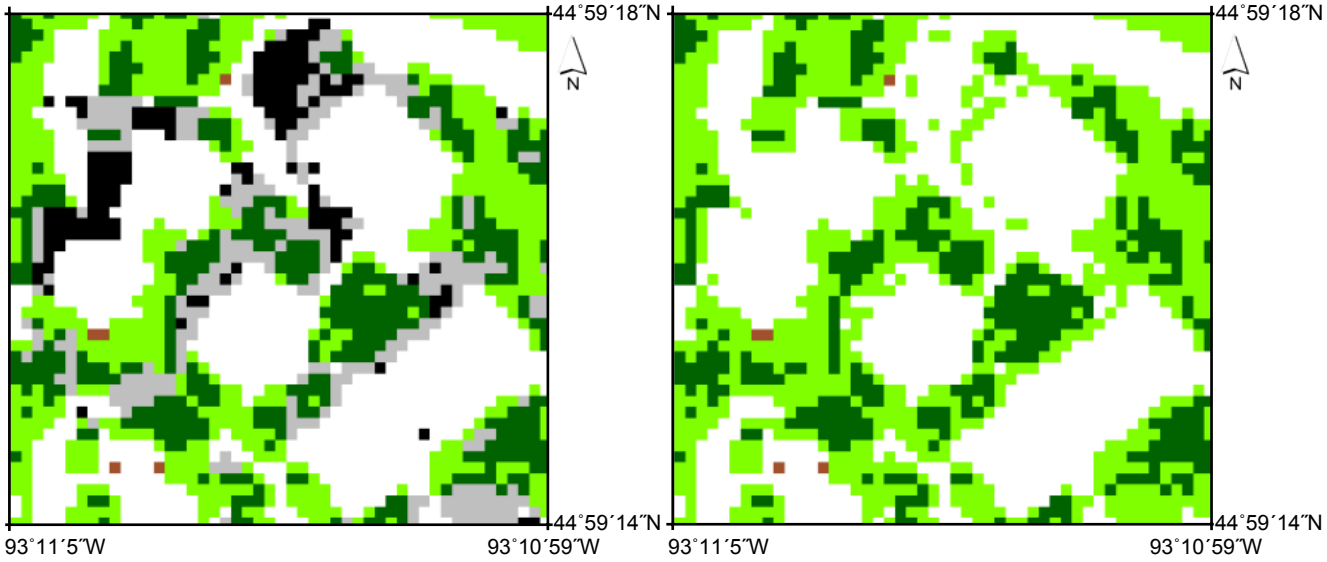

3.2. Turfgrass Net Primary Production

The relationship between fAPAR and NDVI parameterized in this study (Figure 6) performed better than many other fAPAR-NDVI relationships found in the literature [31–33,41,42]. With this relationship, we found that fAPAR will reasonably not exceed 1.0 when NDVI approaches large values. Additionally, the NDVI value for soil surfaces (when fAPAR = 0) derived from this relationship (*i.e.*, 0.22) was closer to that estimated with measured soil reflectances (*i.e.*, 0.31) than if using relationships in the literature (e.g., 0.048 [32]; 0.087 [41]). This also suggests that it may not be appropriate to assign model parameters defined for other vegetation types (e.g., irrigated agricultural crops) to suburban turfgrass or other urban vegetation [43].

Management of turfgrass is highly variable. While turfgrass in some areas such as roadsides receive little attention, golf courses and athletic fields often receive excess water and fertilizer to overcome key growth constraints. Most residential and commercial lawns receive medium amounts of irrigation and fertilization. As a result, the NPP of turfgrass varied significantly across the study area due to different management practices (Figure 7). The annual NPP ranged as low as almost 0 g·C·m^{-2} to as high as 1,301 g·C·m^{-2}. High input turfgrass (e.g., golf course grass) constantly had high productivity and contributed considerably to NPP (>1,000 g·C·m^{-2}·yr^{-1}) while the productivity of low input turfgrass (e.g., roadside turfgrass) was relatively low. The average carbon density (NPP per unit turfgrass cover) on golf course grass (1,100.5 g·C·m^{-2}) was 43% higher than that on regular lawn grass (771.2 g·C·m^{-2}) (Table 4).

Figure 6. The relationship of fraction of absorbed photosynthetically active radiation (fAPAR) to normalized difference vegetation index (NDVI) derived from field biophysical measurements and turfgrass canopy radiation transfer modeling.

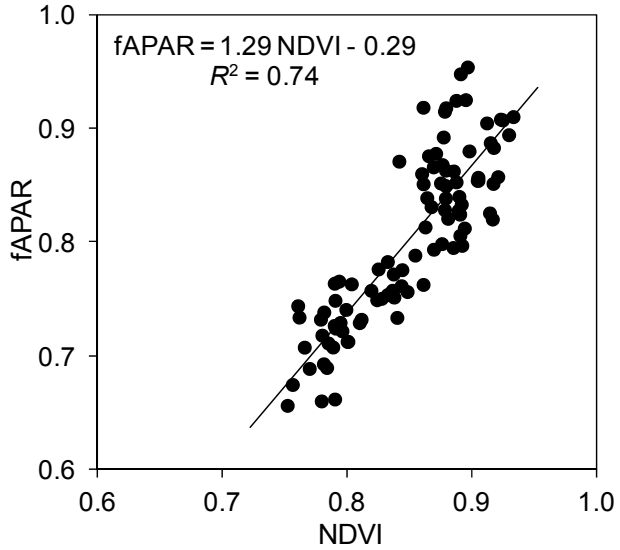

Figure 7. Annual net primary production (NPP) of turfgrass in the study area. Areas in white were not turfgrass and thus were masked.

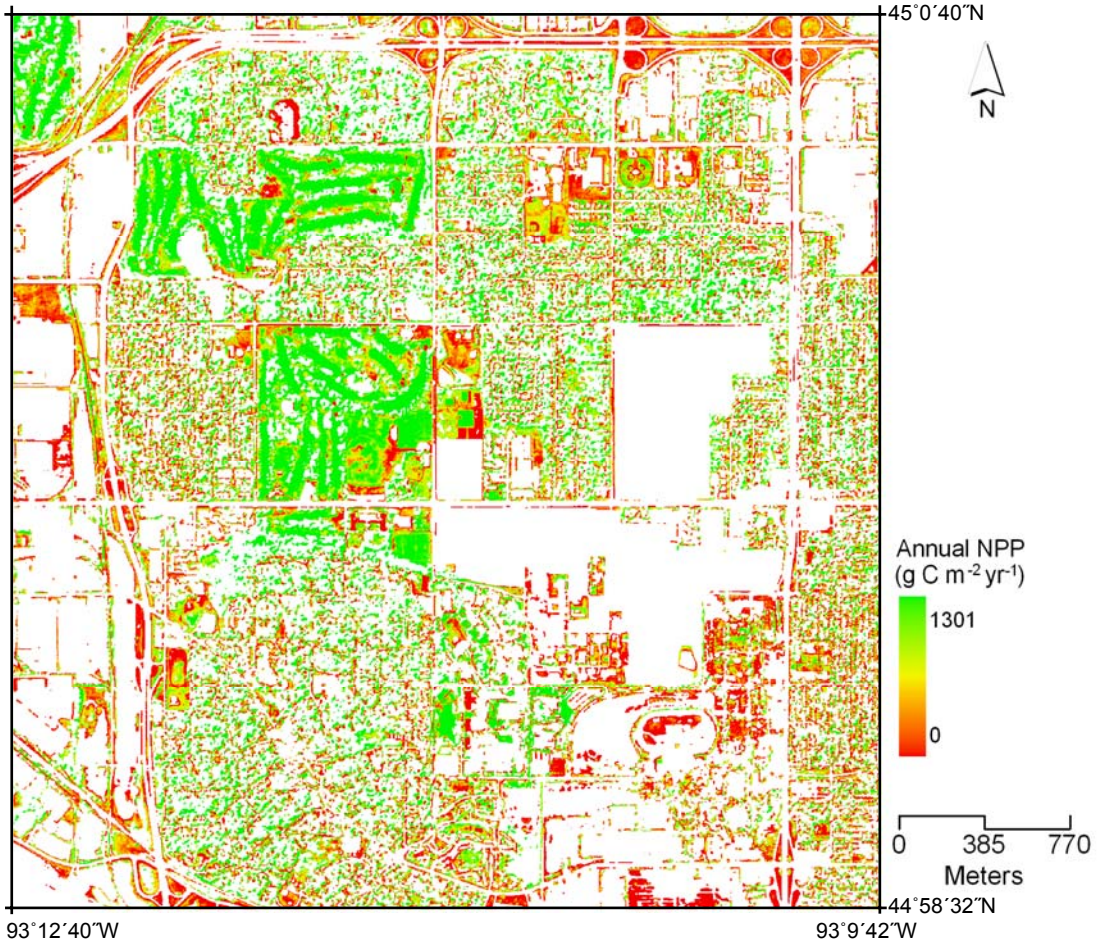

Table 4. Turfgrass (divided into golf course grass and lawn grass) area coverage and estimated average net primary production (NPP) per unit cover and total annual NPP.

	Area (%)	Average NPP per Unit Cover ($g \cdot C \cdot m^{-2} \cdot yr^{-1}$)	Range ($g \cdot C \cdot m^{-2} \cdot yr^{-1}$)	Standard Deviation ($g \cdot C \cdot m^{-2} \cdot yr^{-1}$)	Annual NPP (Tons)
Golf course grass	2.3	1,100.5	225.7–1,301.9	57.2	450
Lawn grass	35.7	771.2	0–1,301.9	324.8	4,250
Total	38.0	796.4	0–1,301.9	330.0	4,700

In addition to the relatively low productivity of lawn grass, the spatial variability of NPP was also greater than that of golf course grass. The standard deviation of the annual NPP of regular lawn grass (324.8 $g \cdot C \cdot m^{-2} \cdot yr^{-1}$) was five times more than that of golf course grass (57.2 $g \cdot C \cdot m^{-2} \cdot yr^{-1}$). However, regular lawn grass still contributed more to the total NPP of the study area because of the larger area coverage of lawn grass (~36% compared with 2% for golf course grass) (Figure 2). Of the total estimated 4,700 tons of carbon absorbed by turfgrass across the study area, 4,250 tons (~90%) were assimilated by lawn grass and 450 tons (~10%) by golf course grass (Table 4).

A sensitivity analysis was also conducted to examine the response of the PEM model to light use efficiencies corresponding to three nitrogen management intensity levels We found that the PEM model was quite sensitive to $\varepsilon_{max}(N)$ values. The average annual NPP would increase by 14.7% or decrease by 30.9% if a constant high $\varepsilon_{max}(N)$ (*i.e.*, 1.08 $g \cdot C \cdot MJ^{-1}$) or low $\varepsilon_{max}(N)$ (*i.e.*, 0.65 $g \cdot C \cdot MJ^{-1}$) was used in the simulation, respectively. The average annual NPP would decrease by 9.6% if a constant medium $\varepsilon_{max}(N)$ (*i.e.*, 0.84 $g \cdot C \cdot MJ^{-1}$) was used. This indicated that differences in nitrogen supplies could cause significant variations of NPP. Thus it was necessary to separate light use efficiency according to nitrogen fertilization levels in estimating turfgrass NPP.

4. Discussion

The analysis indicated a marked high increase in biological carbon fixation of turfgrass compared with native grasslands in the same region (~200 $g \cdot C \cdot m^{-2} \cdot yr^{-1}$ in monoculture) [44], which may be explained by the enhanced management practices such as irrigation and fertilization, and the stimulating effect of clipping on turfgrass [26]. The results are consistent with several other previous studies suggesting that the carbon cycling rate of urban turfgrass is usually higher than other vegetation types. For instance, field measurements of both above-ground and below-ground biomass during a growing season indicated that turfgrass ecosystems were extremely productive with an average NPP of 489 $g \cdot C \cdot m^{-2} \cdot yr^{-1}$ and 792 $g \cdot C \cdot m^{-2} \cdot yr^{-1}$ in separate studies [26,27]. The lab analysis of carbon concentrations of lawn clippings indicated that the collected aboveground biomass ranged from 35 $g \cdot C \cdot m^{-2} \cdot yr^{-1}$ to 540 $g \cdot C \cdot m^{-2} \cdot yr^{-1}$ with an average of 200 $g \cdot C \cdot m^{-2} \cdot yr^{-1}$ [20]. This is equivalent to an average 660 $g \cdot C \cdot m^{-2} \cdot yr^{-1}$ (115–1,800 $g \cdot C \cdot m^{-2} \cdot yr^{-1}$) of annual NPP assuming that clippings remove 30% of total production [6] or an average 1,000 $g \cdot C \cdot m^{-2} \cdot yr^{-1}$ (175–2,700 $g \cdot C \cdot m^{-2} \cdot yr^{-1}$) of annual NPP assuming that clippings remove 20% of total production [27]. The simulation with the Biome-BGC ecosystem model showed that NPP ranged from 22 to 1,063 $g \cdot C \cdot m^{-2} \cdot yr^{-1}$ with an average of 400 $g \cdot C \cdot m^{-2} \cdot yr^{-1}$ [6].

Given the popular hypothesis that biological carbon density is often assumed to be zero or largely neglected once land is considered to be urban [45], the significant NPP of turfgrass found in this study and the high carbon storage of urban trees shown in previous studies [17] reveal an important implication for future land use and land cover change studies. All land use and land cover change, including the conversion of land through the process of urbanization should be accounted for to balance the global carbon budget.

The amount of carbon fixed by turfgrass, however, has to be discounted for potential carbon release in order to fully quantify the carbon balance of urban turfgrass. The potential carbon losses may include soil respiration loss [46] and fossil fuel consumption related to management activities (e.g., through the use of lawn mowers) [23,47]. Carbon sequestration in turf soils occurs at a significant rate, comparable to that of the land placed in the US Conservation Reserve Program [48]. To fully account for the net ecosystem production or NEP of turfgrass, the respiration by soil microbes must be subtracted from the current estimates. The carbon emission in various maintenance activities via fossil fuel combustion may offset some of the biological carbon uptake by turfgrass. Therefore, a complete carbon balance of the whole urban turfgrass ecosystem is needed to include both drivers of fossil fuel emissions and carbon cycling in plants and soils [49].

This study is part of a large project to quantify carbon budget in the urban-suburban ecosystems with two different approaches: satellite remote sensing and eddy covariance flux measurements [50]. While our remote sensing-based estimate of the annual NPP of turfgrass (796.4 $g \cdot C \cdot m^{-2} \cdot yr^{-1}$) falls well within the range reported by other studies of biomass production in lawns (400–1,000 $g \cdot C \cdot m^{-2} \cdot yr^{-1}$) [6,20], we will further compare the result of this study with that of the eddy covariance measurement conducted at the same study site in the future. We caution that the PEM modeling is semi-empirical and will need to be adapted individually to each site.

The accuracy of NPP estimates was also limited by the simplifying assumptions made in the PEM modeling. The results of this study provided a first-order approximation of turfgrass NPP by assuming that the satellite imagery acquired in mid-summer could be used to derive the typical turfgrass canopy conditions throughout the growing season. While we believe this simplification is useful to estimate the overall variation of carbon uptake, the assumption should be used with caution if turfgrass stays in a dormant state for an extended period of time. For intensively managed ecosystems like turfgrass, changes in vegetation surface conditions can be inconsistent and unpredictable. The eddy covariance technique may arguably be the only way that can be used to accurately quantify the temporal dynamic of carbon exchange. However, it has its own challenges in heterogeneous urban landscapes [50]. It is also expensive to operate and mathematically complex. Since these limitations often restrict the effective use of this technique in practice, the method we proposed can provide information to local agencies in developing carbon management programs.

5. Conclusions

We examined the quantities and spatial patterns of the annual NPP of turfgrass in a typical residential neighborhood in the US with a remote sensing-driven PEM approach. A multi-stage image classification scheme was developed to map major land cover types with high resolution QuickBird satellite imagery. Shadows in the remote sensing images, which accounted for about 7% of total land

cover in the study area, were detected and removed by taking advantage of the high radiometric resolution of QuickBird data. The results showed that urban vegetation including turfgrass is an important component of urban-suburban landscapes with significant area coverage. In this suburban neighborhood, urban vegetation accounted for about 60% of the land surface, with about 38% being turfgrass.

As a major vegetation type in US cities, turfgrass can play an important role in helping reduce atmospheric carbon dioxide. The results indicated that, depending on vegetative conditions and management intensity, the productivity of turfgrass was high but with large spatial variability. The greatest NPP was associated with turfgrass in golf courses which received intensive irrigation and fertilization. The average annual NPP of golf course grass (1,100.5 $g \cdot C \cdot m^{-2}$) was 43% higher than that of regular lawn grass (771.2 $g \cdot C \cdot m^{-2}$). But regular lawn grass contributed more to the total NPP due to the larger area coverage, although with higher spatial variability. Only 2% of the land cover was occupied by golf course grass compared with 36% by regular lawn grass. The standard deviation of the annual NPP of regular lawn grass was five times more than that of golf course grass.

Acknowledgments

This research was funded by grants from the University of Minnesota under the Initiative for Renewable Energy and the Environment, the Agricultural Experiment Station, and Department of Forest Resources. The authors wish to acknowledge the support of ground measurements by the Turfgrass Research, Outreach, and Education Center. Special thanks go to Joseph McFadden for advice, Brian Horgan for access to the field site, and David Ruschy for providing meteorological data from the University of Minnesota Climatological Observatory. We also greatly appreciate the constructive suggestions of the editors and three anonymous reviewers. An earlier version of the paper was presented at the 2010 IEEE International Geoscience and Remote Sensing Symposium, 25–30 July 2010, Honolulu, USA.

References

1. UNPD (United Nations Population Division). *World Urbanization Prospects: The 2007 Revision*; United Nations Department of Economic and Social Affairs: New York, NY, USA, 2008.
2. White, E.M.; Morzillo, A.T.; Aliga, R.J. Past and projected rural land conversion in the US at state, regional, and national levels. *Landscape Urban Plan.* **2009**, *89*, 37-48.
3. Johnson, M.P. Environmental impacts of urban sprawl: A survey of the literature and proposed research agenda. *Environ. Plann. A* **2001**, *33*, 717-735.
4. Grimm, N.B.; Faeth, S.H.; Golubiewski, N.E.; Redman, C.L.; Wu, J.; Bai, X.; Briggs, J.M. Global change and the ecology of cities. *Science* **2008**, *319*, 756-760.
5. Nowak, D.J.; Noble, M.H.; Sisinni, S.M.; Dwyer, J.F. Assessing the US urban forest resources. *J. Forest.* **2001**, *99*, 37-42.
6. Milesi, C.; Running, S.W.; Elvidge, C.D.; Dietz, J.B.; Tuttle, B.T.; Nemani, R.R. Mapping and modeling the biogeochemical cycling of turf grasses in the United States. *Environ. Manage.* **2005**, *36*, 426-438.

7. Tzoulas, K.; Korpela, K.; Venn, S.; Yli-Pelkonen, V.; Kaźmiercak, A.; Niemela, J.; James, P. Promoting ecosystem and human health in urban areas using greenspace infrastructure: A literature review. *Landscape Urban Plan.* **2007**, *81*, 167-178.
8. Bolund, P.; Hunhammar, S. Ecosystem services in urban areas. *Ecol. Econ.* **1999**, *29*, 293-301.
9. Spronken-Smith, R.A.; Oke, T.R.; Lowry, W.P. Advection and the surface energy balance across an irrigated urban park. *Int. J. Climatol.* **2000**, *20*, 1033-1047.
10. Escobedo, F.J.; Nowak, D.J. Spatial heterogeneity and air pollution removal by an urban forest. *Landscape Urban Plan.* **2009**, *90*, 102-110.
11. Pauleit, S.; Duhme, F. Assessing the environmental performance of landcover types for urban planning. *Landscape Urban Plan.* **2000**, *52*, 1-20.
12. Gehrt, S.D.; Chelsvig, J.E. Species-specific patterns of bat activity in an urban landscape. *Ecol. Appl.* **2004**, *14*, 625-635.
13. Bondeau, A.; Smith, P.C.; Zaehle, S.; Schaphoff, S.; Lucht, W.; Cramer, W.; Gerten, D.; Lotze-Campen, H.; Muller, C.; Reichstein, M.; Smith, B. Modelling the role of agriculture for the 20th century global terrestrial carbon balance. *Global Change Biol.* **2007**, *13*, 679-706.
14. Vuichard, N.; Ciais, P.; Viovy, N.; Calanca, P.; Soussana, J.-F. Estimating the greenhouse gas fluxes of European grasslands with a process-based model: 2. Simulations at the continental level. *Global Biogeochem. Cy.* **2007**, *21*, doi: 10.1029/2005GB002612.
15. Mckinley, D.C.; Ryan, M.G.; Birdsey, R.A.; Giardina, C.P.; Harmon, M.E.; Heath, L.S.; Houghton, R.A.; Jackson, R.B.; Morrison, J.F.; Murray, B.C.; Pataki, D.E.; Skog, K.E. A synthesis of current knowledge on forests and carbon storage in the United States. *Ecol. Appl.* **2011**, *21*, 1902-1924.
16. Potere, D.; Schneider, A. A critical look at representations of urban areas in global maps. *GeoJournal* **2007**, *69*, 55-80.
17. Nowak, D.J.; Crane, D.E. Carbon storage and sequestration by urban trees in the USA. *Environ. Pollut.* **2002**, *116*, 381-389.
18. Kaye, J.P.; Mcculley, R.L.; Burke, I.C. Carbon fluxes, nitrogen cycling, and soil microbial communities in adjacent urban, native and agricultural ecosystems. *Global Change Biol.* **2005**, *11*, 575-587.
19. Churkina, G. Modeling the carbon cycle of urban systems. *Ecol. Model.* **2008**, *216*, 107-113.
20. Golubiewski, N.E. Urbanization increases grassland carbon pools: Effects of landscaping in Colorado's Front Range. *Ecol. Appl.* **2006**, *16*, 555-571.
21. Zhao, T.; Brown, D.G.; Bergen, K.M. Increasing gross primary production (GPP) in the urbanizing landscapes of southeastern Michigan. *Photogramm. Eng. Remote Sensing* **2007**, *73*, 1159-1168.
22. Imhoff, M.L.; Bounoua, L.; DeFries, R.; Lawrence, W.T.; Stutzer, D.; Tucker, C.J.; Ricketts, T. The consequences of urban land transformation on net primary productivity in the United States. *Remote Sens. Environ.* **2004**, *89*, 434-443.
23. Jo, H.-K.; McPherson, E.G., Carbon storage and flux in urban residential greenspace. *J. Environ. Manage.* **1995**, *45*, 109-133.

24. Pickett, S.T.A.; Cadenasso, M.L.; Grove, J.M.; Nilon, C.H.; Pouyat, R.V.; Zipperer, W.C.; Costanza, R. Urban ecological systems: Linking terrestrial ecological, physical, and socioeconomic components of metropolitan areas. *Ann. Rev. Ecol. Evol. S.* **2001**, *32*, 127-157.
25. Davies, Z.G.; Edmondson, J.L.; Heinemeyer, A.; Leake, J.R.; Gaston, K.J. Mapping an urban ecosystem service: Quantifying above-ground carbon storage at a city-wide scale. *J. Appl. Ecol.* **2011**, *48*, 1125-1134.
26. Falk, J.H. Energetics of a suburban lawn ecosystem. *Ecology* **1976**, *57*, 141-150.
27. Falk, J.H. The primary productivity of lawns in a temperate environment. *J. Appl. Ecol.* **1980**, *17*, 689-695.
28. Cadenasso, M.L.; Pickett, S.T.A.; Schwarz, K. Spatial heterogeneity in urban ecosystems: Reconceptualizing land cover and a framework for classification. *Front. Ecol. Environ.* **2007**, *5*, 80-88.
29. Moskal, L.M.; Styers, D.M.; Halabisky, M. Monitoring urban tree cover using object-based image analysis and public domain remotely sensed data. *Remote Sens.* **2011**, *3*, 2243-2262.
30. Dare, P.M. Shadow analysis in high-resolution satellite imagery of urban areas. *Photogramm. Eng. Remote Sensing* **2005**, *71*, 169-177.
31. Veroustraete, F.; Sabbe, H.; Eerens, H. Estimation of carbon mass fluxes over Europe using the C-Fix model and Euroflux data. *Remote Sens. Environ.* **2002**, *83*, 376-399.
32. Seaquist, J.W.; Olsson, L.; Ardö, J. A remote sensing-based primary production model for grassland biomes. *Ecol. Model.* **2003**, *169*, 131-155.
33. Sims, D.A.; Rahman, A.F.; Cordova, V.D.; El-Masri, B.Z.; Baldocchi, D.D.; Flanagan, L.B.; Goldstein, A.H.; Hollinger, D.Y.; Misson, L.; Monson, R.; *et al*. On the use of MODIS EVI to assess gross primary productivity of North American ecosystems. *J. Geophys. Res.* **2006**, *111*, doi: 10.1029/2006JG000162.
34. Zhao, M.; Running, S.W. Remote Sensing of Terrestrial Primary Production and Carbon Cycle. In *Advances in Land Remote Sensing: System, Modeling, Inversion and Application*, 1st ed.; Liang, S., Ed.; Springer: New York, NY, USA, 2008; pp. 423-444.
35. McCallum, I.; Wagner, W.; Schmullius, C.; Shvidenko, A.; Obersteiner, M.; Fritz, S.; Nilsson, S. Satellite-based terrestrial production efficiency modeling. *Carbon Balance Manage.* **2009**, *4*, doi: 10.1186/1750-0680-4-8.
36. Wu, J.; Wang, D.; Bauer, M.E. Image-based atmospheric correction of QuickBird imagery of Minnesota cropland. *Remote Sens. Environ.* **2005**, *99*, 315-325.
37. Duda, R.O.; Hart, P.E. *Pattern Classification and Scene Analysis*, 1st ed.; Wiley: New York, NY, USA, 1973.
38. Robson, M.J.; Parsons, A.J. Nitrogen deficiency in small closed communities of S24 ryegrass. I. photosynthesis, respiration, dry matter production and partition. *Ann. Bot.-London* **1978**, *42*, 1185-1197.
39. Bremer, D.J.; Ham, J.M. Measurement and partitioning of in situ CO_2 fluxes in turfgrasses using a pressurized chamber. *Agron. J.* **2005**, *97*, 627-632.
40. Wu, J.; Wang, D.; Bauer, M.E. Assessing broadband vegetation indices and QuickBird data in estimating leaf area index of corn and potato canopies. *Field Crop. Res.* **2007**, *102*, 33-42.

41. Asrar, G.E.; Fuchs, M.; Kanemasu, E.T.; Hatfield, J.L. Estimating absorbed photosynthetic radiation and leaf area index from spectral reflectance in wheat. *Agron. J.* **1984**, *76*, 300-306.
42. Myneni, R.B.; Williams, D.L. On the relationship between FAPAR and NDVI. *Remote Sens. Environ.* **1994**, *49*, 200-211.
43. As-syakur, A.R.; Osawa, T.; Adnyana, I.W.S. Medium spatial resolution satellite imagery to estimate gross primary production in an urban area. *Remote Sens.* **2010**, *2*, 1496-1507.
44. Tilman, D.; Reich, P.B.; Knops, J.; Wedin, D.; Mielke, T.; Lehman, C. Diversity and productivity in a long-term grassland experiment. *Science* **2001**, *294*, 943-845.
45. Dyson, K.E.; Mobbs, D.C.; Milne, R. Annual Inventory Estimates for the UK (WP 1.1). In *Inventory and Projections of UK Emissions by Sources and Removals by Sinks due to Land Use, Land Use Change and Forestry*; Dyson, K.E., Ed.; Department for the Environment, Food and Rural Affairs: London, UK, 2009; pp. 13-49.
46. Pouyat, R.V.; Yesilonis, I.D.; Nowak, D.J. Carbon storage by urban soils in the United States. *J. Environ. Qual.* **2006**, *35*, 1566-1575.
47. Townsend-Small, A.; Czimczik, C.I. Carbon sequestration and greenhouse gas emissions in urban turf. *Geophys. Res. Lett.* **2010**, *37*, doi: 10.1029/2009GL041675.
48. Qian, Y.; Follett, R.F. Assessing soil carbon sequestration in turfgrass systems using long-term soil testing data. *Agron. J.* **2002**, *94*, 930-935.
49. Pataki, D.E.; Alig, R.J.; Fung, A.S.; Golubiewski, N.E.; Kennedy, C.A.; Mcpherson, E.G.; Nowak, D.J.; Pouyat, R.V.; Romero Lankao, P. Urban ecosystems and the North American carbon cycle. *Global Change Biol.* **2006**, *12*, 2092-2102.
50. Hiller, R.V.; McFadden, J.P.; Kljun, N. Interpreting CO_2 fluxes over a suburban lawn: The influence of traffic emissions. *Bound.-Lay. Meteorol.* **2011**, *138*, 215-230.